

5. DATA REPORT: SULFIDE MINERAL CHEMISTRY AND PETROGRAPHY FROM BENT HILL, ODP MOUND, AND TAG MASSIVE SULFIDE DEPOSITS¹

Darren Lawrie² and D. Jay Miller^{2,3}

ABSTRACT

Sulfide mineral major and trace element analyses were performed on more than 50 polished slabs representing mineralization from three seafloor hydrothermal massive sulfide deposits. Samples from the Bent Hill and ODP Mound massive sulfide deposits, both on the Juan de Fuca Ridge, can be contrasted with samples from the Trans-Atlantic Geotraverse (TAG) hydrothermal mound on the Mid-Atlantic Ridge. The massive sulfide at Bent Hill is predominantly pyrite and pyrrhotite, with increasing amounts of copper-bearing sulfide minerals at the base of the massive sulfide body and through the stockwork to an interval 200 m below seafloor that hosts high copper mineralization (Deep Copper Zone). ODP Mound contains much more abundant sphalerite and copper-bearing sulfides as compared to either Bent Hill or TAG, which are predominantly pyrite with much less abundant chalcopyrite. Copper-bearing sulfides from the Deep Copper Zone beneath Bent Hill and the lowest sampled interval of ODP Mound are petrographically and chemically similar, but distinct from copper-bearing minerals higher in either sequence.

INTRODUCTION

Of the four economically important categories of ancient massive sulfide deposits that are known to have modern seafloor analogs, two

¹Lawrie, D., and Miller, D.J., 2000. Data report: Sulfide mineral chemistry and petrography from Bent Hill, ODP Mound, and TAG massive sulfide deposits. In Zierenberg, R.A., Fouquet, Y., Miller, D.J., and Normark, W.R. (Eds.), *Proc. ODP, Sci. Results*, 169, 1-34 [Online]. Available from World Wide Web: <http://www-odp.tamu.edu/publications/169_SR/VOLUME/CHAPTERS/SR169_05.PDF>. [Cited YYYY-MM-DD]

²Ocean Drilling Program, Texas A&M University, 1000 Discovery Drive, College Station TX 77845-9547, USA.

³Correspondence author:
miller@odpemail.tamu.edu

have been the focus of recent Ocean Drilling Program (ODP) expeditions. In 1994 we sampled what is potentially the simplest system at the Trans-Atlantic Geotraverse (TAG) hydrothermal mound where only basaltic rock is present for reaction with hydrothermal fluid. In 1991 and again in 1996, ODP targeted a more complex system where terrigenous sediments and basaltic rocks are available for reaction with hydrothermal fluid (Juan de Fuca). As part of an ongoing study related to the Re-Os isotope systematics of these two systems, we present data from petrographic studies and compositional analysis of sulfide minerals as a reference for other authors publishing results from sampling these two hydrothermal areas.

GEOLOGIC BACKGROUND

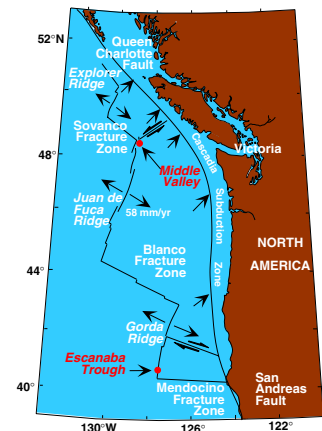
Juan de Fuca

The Juan de Fuca Ridge is a medium-rate spreading center located in the northeastern Pacific Ocean a few hundred kilometers west of Vancouver Island (Fig. F1). On the northernmost part of the ridge there is an ~50-km-long rift segment known as Middle Valley. Middle Valley is one of the branches on the northernmost Juan de Fuca Ridge that constitutes a ridge-transform-transform unstable triple junction with the Nootka Fault and Sovanco Fracture Zone (Davis and Villinger, 1992). Owing to its proximity to the North American craton and consequent rapid sedimentation rates, Middle Valley is an easily accessible representative of sediment-covered rifts. Volcanism in the area of interest is expressed as a series of sills intercalated within a sedimentary package several hundred meters thick and composed of turbidite and hemipelagic sediment (Davis, Mottl, Fisher, et al., 1992). Part of the drilling operation during Leg 169 at Middle Valley was focused on hydrothermal massive sulfide deposits exposed on the seafloor. Specifically targeted were the Bent Hill Massive Sulfide (BHMS) deposit at $48^{\circ}26.0'N$, $128^{\circ}40.9'W$ (2423 m below sea level [mbsl]) and ODP Mound deposit at $48^{\circ}25.8'N$, $128^{\circ}40.9'W$ (2443 mbsl). The BHMS deposit was initially drilled during Leg 139. Hole 856H was cored to a depth of 93.8 m below seafloor (mbsf) but was abandoned because of unstable hole conditions. During Leg 169, this hole was reentered and deepened to 500 mbsf. ODP Mound (Hole 1035H) is located ~300 m south of the BHMS deposit and was cored to a depth of 247.9 mbsf.

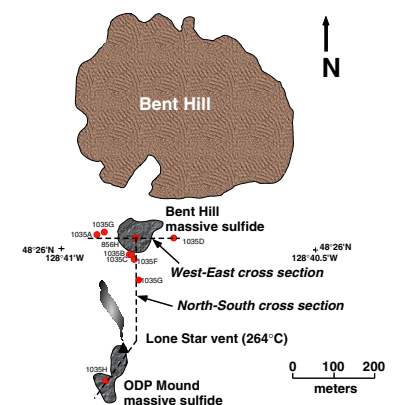
Surface Morphology and Stratigraphy of the BHMS and ODP Mound Deposits

Bent Hill is one of a series of small uplifted sediment mounds that are strung out in a line roughly parallel to the eastern wall of Middle Valley (Davis, Mottl, Fisher, et al., 1992). The BHMS deposit outcrops ~100 m south of Bent Hill and has a roughly circular shape in plan view (Fig. F2). ODP Mound outcrops ~300 m south of the BHMS deposit, and although it has an irregular shape, it lies along a line that is continuous with the linear ridge along the west side of Bent Hill and that passes through the BHMS deposit. This alignment suggests a subsurface fault imaged by a 3.5-kHz sub-bottom profiler (R. Zierenberg, pers. comm., 1999) and might be partially responsible for the location of the BHMS and ODP Mound deposits, but no fault has been seismically imaged (Fouquet, Zierenberg, Miller, et al., 1998). Until Leg 169, the only report

F1. Location map of Middle Valley on the Juan de Fuca Ridge. p. 10.



F2. Plan view of the BHMS and ODP Mound deposits, p. 11.



of active hydrothermal upwelling was from a small vent on the northern part of ODP Mound (Fig. F2). Subsequent submersible observations located a second vent near Hole 1035H (R. Zierenberg, pers. comm., 1999).

The stratigraphy of the BHMS deposit (Fig. F3) consists of a thin layer of unconsolidated clastic sulfides overlying a >90-m-thick massive sulfide body (Davis, Mottl, Fisher, et al., 1992). The massive sulfide (dominantly pyrrhotite and pyrite) is underlain by a sulfide feeder zone (100–200 mbsf) with predominantly subvertical veins that diminish in abundance downward. A copper-rich sulfide mineralized zone was cored at the base of the feeder zone with exclusively subhorizontal veining (Deep Copper Zone). The sulfide-bearing zone is underlain by interbedded and variably altered hemipelagic and turbiditic sediments, a basaltic sill-sediment complex, and, finally, basaltic flows (Fouquet, Zierenberg, Miller, et al., 1998).

Hole 1035H was drilled near the southernmost peak of ODP Mound (Fig. F2). The stratigraphy of this deposit is markedly different than that of the BHMS deposit. Although ODP Mound is capped by a thin layer of clastic sulfides, the subsurface is characterized by a series of at least three massive sulfide bodies interrupted by densely to sparsely veined feeder zones. The lowermost sulfide mineralization recovered from ODP Mound appears to be similar to the lowermost mineralized sediments recovered from the BHMS deposit (abundant copper-rich sulfides), but copper mineralization is more common throughout the ODP Mound section than in the massive sulfide body at the BHMS deposit (Fouquet, Zierenberg, Miller, et al., 1998).

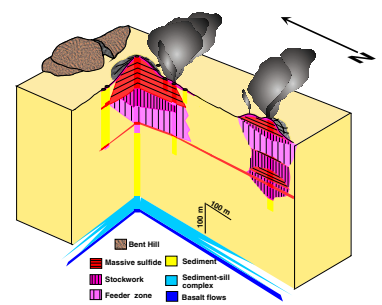
TAG

The TAG hydrothermal mound is located at 26°8.2'N and 44°49.5'W along the eastern margin of the Mid-Atlantic Ridge axial valley. In plan view, the mound has a roughly circular geometry (Fig. F4) and 30–50 m of relief and is ~200 m in diameter. At a water depth of ~3650 mbsl, the mound is built on 100-k.y.-old oceanic crust (Kleinrock et al., 1996). Karson and Rona (1990) have reported that the location of the mound may be influenced by the intersection of axis-parallel faults with transverse or oblique faults. In a recent study, Bohnenstiehl and Kleinrock (1998) report a substantial number of fissures on the seafloor near TAG Mound do have an oblique orientation relative to the ridge axis, but, based on geometric relationships, most of these appear to be shallow features. Uranium/thorium dating on samples from the mound suggest hydrothermal activity has taken place episodically over the last 40 to 50 k.y. (Lalou et al., 1995).

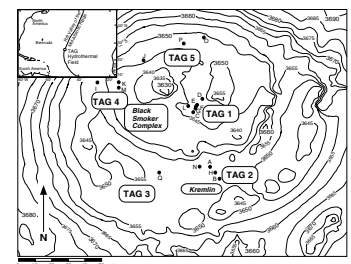
Surface Morphology and Stratigraphy of the TAG Massive Sulfide Deposit

Active hydrothermal venting on TAG Mound has an asymmetric distribution. The mound hosts black and white smoker chimneys, as well as nearly ubiquitous diffuse hydrothermal fluid venting. West of the central part of the mound, there is a 20- to 30-m diameter area of black smoker chimneys 10–15 m high discharging hydrothermal fluids at temperatures on the order of 370°C. This cluster of chimneys is encompassed by an upper terrace at 3644 mbsl, which is in turn surrounded by a lower terrace at 3650 mbsl. On the lower terrace, southeast of the black smoker chimneys, is a white smoker chimney complex known as

F3. Schematic box diagram showing the stratigraphy of the BHMS and ODP Mound deposits, p. 12.



F4. Location map of drill sites on the TAG hydrothermal mound, p. 13.



the Kremlin area. These white smokers are relatively small (1–2 m) and sphalerite rich, and they discharge fluids between 260° and 300°C (Edmond et al., 1995; Mills and Elderfield, 1995; Tivey et al., 1995).

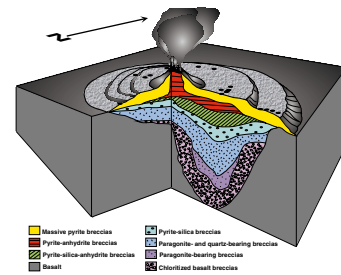
The surface architecture of TAG Mound is in a constant state of flux. According to Rona and Von Herzen (1996), through personal communication with a dive team that had visited TAG and made visual observations via submersible in 1986 and then again in 1990, the mound appeared to be so different that the team questioned whether it was the same mound. Locating markers that were emplaced in 1986, however, resolved this question. In 1986 at the black smoker complex, chimneys towered tens of meters in height and were discharging a thick cloud of black hydrothermal fluid. In the Kremlin area, a cloud of white hydrothermal fluid was observed emanating from tens of chimneys a few meters in height. During the 1990 revisit, the mound appeared to exhibit less hydrothermal activity and reduced chimney size at both the black smoker complex and Kremlin area. This attests to the time scale of fluctuation in activity of hydrothermal activity at TAG.

The diverse internal structure of the TAG Mound was the focus of an ODP drilling expedition (Humphris, Herzig, Miller, et al., 1996). During Leg 158, five different localities (TAG-1 through TAG-5, Fig. F4) on the mound were drilled with the intent of investigating the mound's subsurface three-dimensional variability. The mound is composed of a complex assemblage of sulfide, anhydrite, and siliceous breccias. The uppermost layer of hydrothermal precipitates is made up of massive pyrite and pyrite breccias. Beneath this is a zone of anhydrite-pyrite breccias, underlain in turn by pyrite-silica breccias. The sulfide-rich breccias overlie a stockwork zone that occupies a majority of the vertical extent of the TAG Mound drilled during Leg 158. The stockwork section has been divided into three zones—an upper paragonite and quartz-bearing zone, an intermediate paragonite-bearing stockwork, and a lower chloritic stockwork (Fig. F5). At shallow depths on the fringes of the mound and beneath the hydrothermal precipitates is basaltic basement that is variably, but generally moderately to only slightly, altered (Humphris et al., 1995).

METHODS

Mineral identifications were made from examination of more than 50 polished slabs and thin sections. Photomicroscopy was performed with a Zeiss Axioscope, and, unless otherwise noted, sections were carbon coated to enhance contrast. Quantitative analyses of sulfide minerals were performed using a Cameca Camebax SX50 electron microprobe in the Department of Geology and Geophysics at Texas A&M University. Operating conditions were 15 kV with a beam current of 30 nA, a counting time of 30 s, and a 1-μm focused beam. Natural sulfide standards from Chuck Taylor (FeS_2 , ZnS , PbS , GaAs , and Sb_2Te_3) were used for calibration of Fe, S, Zn, Pb, As, and Sb, respectively, and routinely analyzed as unknowns to check for drift. Pure Cu wire (also analyzed as a drift standard), Ni, Co, and Au were used as calibration standards. These analyses were performed as a first-pass filter to identify minerals of interest for more detailed trace element analysis. The data are presented here in Tables T1, T2, T3, T4, and T5 as a reference and to supplement other data sets generated as part of postcruise research from Leg 169.

F5. Schematic box diagram showing the stratigraphy of the TAG hydrothermal mound, p. 14.



T1. Sulfide mineral compositions from Juan de Fuca Ridge, p. 20.

T2. Sulfide mineral compositions from TAG, p. 22.

T3. Sulfide mineral analysis data table for Bent Hill, p. 24.

T4. Sulfide mineral analysis data table for ODP Mound, p. 27.

T5. Sulfide mineral analysis data table for TAG, p. 31.

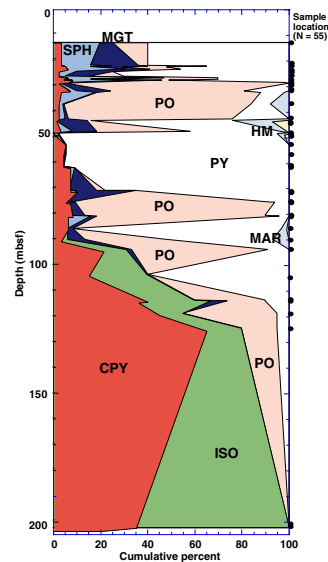
RESULTS AND DISCUSSION

During Leg 169, the general stratigraphy of the Bent Hill deposit was defined (Fouquet, Zierenberg, Miller, et al., 1998). We also recognized the marked difference in mineralogy between the massive sulfide body and the Deep Copper Zone; in particular the abundance of isocubanite and chalcopyrite was significantly higher in the Deep Copper Zone than had been reported from any part of the massive sulfide body. The massive sulfide at Bent Hill is predominantly pyrite and pyrrhotite, with much lower abundance of sphalerite, chalcopyrite, and magnetite (Fig. F6). The relative proportions of pyrite and pyrrhotite vary antithetically; intervals rich in pyrite do not contain much pyrrhotite and vice versa. Figure F6 is an expansion of a similar graphic presented by Krasnov et al. (1994). Sulfide and magnetite abundance is normalized to 100% and plotted against depth in the section, including data from the additional penetration achieved during Leg 169. Note that in this graphic there are no data between ~125 and 200 mbsf, so the proportions of chalcopyrite and isocubanite in this interval are not known. The amount of sulfide mineralization in this interval is much less than 5% of the recovered core, but our visual inspection of the thin (<2 mm in most cases) sulfide veins and small nodules in the interval between 125 and 200 mbsf agree with the descriptions reported from Leg 169, where chalcopyrite (or at least copper-rich sulfide) is much more abundant over this interval than any other sulfide, and pyrrhotite is much more common than pyrite. Additionally, we note that the greater abundance of copper-bearing minerals is not restricted to the Deep Copper Zone, but, in fact, copper enrichment starts in the base of the massive sulfide body (present in Sample 169-856H-19R-1, 60–64 cm, from 94 mbsf), and there is significant copper enrichment in the upper part of the stockwork (Samples 169-856H-20R-1, 32–36 cm; 21R-1, 54–58 cm; 21R-1, 80–84 cm; 22R-2, 57–60 cm; and 23R-1, 94–98 cm).

The principal difference between the two massive sulfide deposits drilled during Leg 169 is the presence of multiple massive sulfide horizons separated by smaller, less well developed stockwork zones in ODP Mound (see Fig. F3). There is also a distinct difference in the sulfide minerals present. Sphalerite is much more abundant in ODP Mound, and copper-bearing sulfides are also common throughout the deposit (Fouquet, Zierenberg, Miller, et al., 1998). Our data indicate that there is also a difference in the chemistry of the individual massive sulfide bodies in ODP Mound (Tables T1, T4). Sphalerites from the uppermost massive sulfide body (recovered in the interval between 9 and 26 mbsf) are the most iron rich, on average nearly 20 wt% Fe. Sphalerite from the thin massive sulfide body recovered from between 75 and 84 mbsf has slightly lower iron enrichment (~16 wt% Fe). The lowermost massive sulfide body, recovered from between 127 and 160 mbsf, has variable (9–11 wt% Fe) but generally lower iron enrichment than the upper two massive sulfide intervals. Zinc content in isocubanite is high (nearly 1 wt%) throughout the deposit, except for samples from the lowest part of the section. In contrast to all the Juan de Fuca data, all our sulfide mineral analyses from the TAG hydrothermal mound are remarkably uniform, despite sampling from various depths and from several locations around the deposit (Tables T2, T5).

The lateral extent of the Deep Copper Zone is a subject of some speculation in the literature from Leg 169 (Fouquet, Zierenberg, Miller, et al., 1998). During the cruise, we surmised that the presence of copper

F6. Changes in sulfide mineral and magnetite concentration, p. 15.



mineralization at the same depth below sea level at both the BHMS deposit and ODP Mound indicated this may be a continuous horizon. Figure F7 illustrates the similarity in appearance of isocubanite from the Deep Copper Zone sampled at both the BHMS deposit and ODP Mound as well as from the base of the BHMS deposit. Elongated but relatively broad lamellae of chalcopyrite account for 20% to 30% of the exposed surface area of isocubanite. Although isocubanite from the Deep Copper Zone sampled at the BHMS deposit and ODP Mound are geochemically indistinguishable (see Table T1, Sample 169-1035H-19R-1, 58–62 cm; Table T2, Sample 169-856H-31R-2, 1–5 cm), isocubanite from the base of the BHMS deposit is significantly richer in iron and zinc.

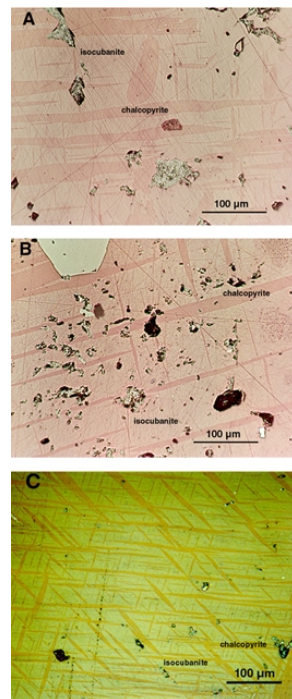
Chalcopyrite disease (Barton and Bethke, 1987) was reported in samples from ODP Mound, although the intensity of this malady is highly variable even within a single sample. Figure F8 illustrates the morphology and distribution of chalcopyrite inclusions in sphalerite from Sample 169-1035H-16R-2. Figure F9 illustrates differences in paragenetic relationships in the massive sulfide bodies of ODP Mound. In Figure F9A, a corona of pyrrhotite surrounds anhedral sphalerite, which in turn exhibits variable amounts of exsolved chalcopyrite. Figure F9B shows the common relationship in these samples of massive pyrite dissected by anastomosing veins of pyrrhotite. It is also common to see pyrrhotite veins cutting pyrite veins, which cut through large anhedral sphalerite crystals (Fig. F9C). Rarely there is evidence of early pyrite crystallization as euhedral inclusions in sphalerite (Fig. F9D). More complex paragenetic histories are present in other samples, as shown in Figure F9E from a sample in the uppermost massive sulfide horizon. Vermicular embayments around the margin of chalcopyrite are in places filled with pyrite, and the entire grain is armored by sphalerite. Figure F9F (same horizon as the sample in Fig. F9E) has a similar mineral assemblage. Irregularly shaped but surrounded chalcopyrite is riddled with pyrite veins and inclusions and surrounded by sphalerite that also has pyrite-filled embayments.

We performed several analyses on grains that had anomalous appearances in reflected light. Although most of these resulted in totals significantly <100%, a few analyses were of submicroscopic inclusions of intimately intermixed phases. Listed under “Anomalies” in Table T1, these include grains that appear to be finely intergrown chalcopyrite and sphalerite. The analyses equate to a 75/23/2 mixture of chalcopyrite, pyrite, and sphalerite, and a 50/25/22/3 mixture of chalcopyrite, pyrite, pyrrhotite, and sphalerite, respectively. Note that these analyses were performed with a focused 1- μm beam, indicating the intimacy of these intergrowths. The last two analyses are from a euhedral galena inclusion in sphalerite (Fig. F10). Although petrographically there is no evidence of microscopic inclusions in the galena, these analyses included 12% and 7% antimony.

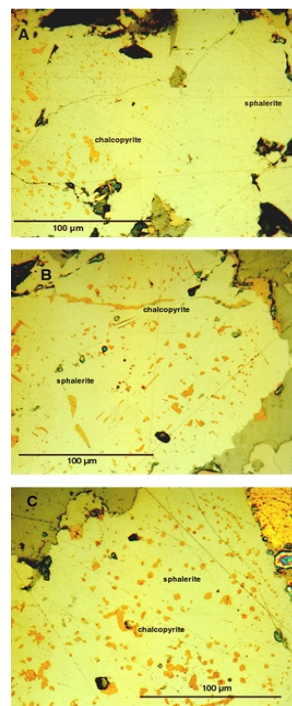
ACKNOWLEDGMENTS

This study was funded through the United States Science Support Program. The authors wish to thank the Ocean Drilling Program for providing the samples and F. Barriga and R. Zierenberg, who provided thorough and thoughtful reviews of the manuscript.

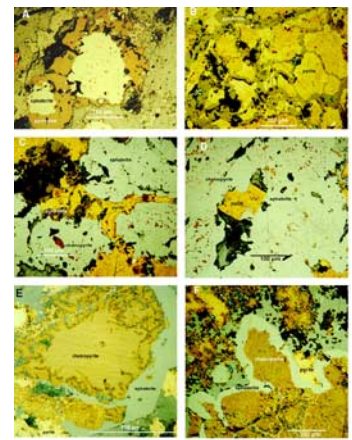
F7. Photomicrographs of isocubanite and chalcopyrite, p. 16.



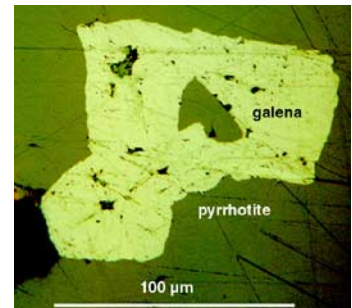
F8. Photomicrographs of chalcopyrite disease in sphalerite, p. 17.



F9. Photomicrographs illustrating paragenetic relationships in ODP Mound massive sulfides, p. 18.



F10. Photomicrograph of euhe-
dral galena inclusion in sphalerite,
p. 19.



REFERENCES

- Barton, P.B., Jr., and Bethke, P.M., 1987. Chalcopyrite disease in sphalerite: pathology and epidemiology. *Am. Mineral.*, 72:451–467.
- Bohnenstiehl, D.R., and Kleinrock, M.C., 1998. The orientation and size of fissures near the TAG Active Mound, 26 degrees north on the Mid-Atlantic Ridge. *Eos*, F44.
- Davis, E.E., Mottl, M.J., Fisher, A.T., et al., 1992. *Proc. ODP, Init. Repts.*, 139: College Station, TX (Ocean Drilling Program).
- Davis, E.E., and Villinger, H., 1992. Tectonic and thermal structure of the Middle Valley sedimented rift, northern Juan de Fuca Ridge. In Davis, E.E., Mottl, M.J., Fisher, A.T., et al., *Proc. ODP, Init. Repts.*, 139: College Station, TX (Ocean Drilling Program), 9–41.
- Edmond, J.M., Campbell, A.C., Palmer, M.R., German, C.R., Klinkhammer, G.P., Edmonds, H.N., Elderfield, H., Thompson, G., and Rona, P., 1995. Time-series studies of vent fluids from the TAG and MARK sites (1986, 1990): Mid-Atlantic Ridge: a new solution chemistry model and a mechanism for Cu/Zn zonation in massive sulfide ore bodies. In Parson, L.M., Walker, C.L., and Dixon, D.R. (Eds.), *Hydrothermal Vents and Processes*. Geol. Soc. Spec. Publ. London, 87:77–86.
- Fouquet, Y., Zierenberg, R.A., Miller, D.J., et al., 1998. *Proc. ODP, Init. Repts.*, 169: College Station, TX (Ocean Drilling Program).
- Humphris, S.E., Herzig, P.M., Miller, D.J., Alt, J.C., Becker, K., Brown, D., Brügmann, G., Chiba, H., Fouquet, Y., Gemmell, J.B., Guerin, G., Hannington, M.D., Holm, N.G., Honnorez, J.J., Itturino, G.J., Knott, R., Ludwig, R., Nakamura, K., Petersen, S., Reysenbach, A.-L., Rona, P.A., Smith, S., Sturz, A.A., Tivey, M.K., and Zhao, X., 1995. The internal structure of an active sea-floor massive sulphide deposit. *Nature*, 377:713–716.
- Humphris, S.E., Herzig, P.M., Miller, D.J., et al., 1996. *Proc. ODP, Init. Repts.*, 158: College Station, TX (Ocean Drilling Program).
- Karson, J.A., and Rona, P.A., 1990. Block tilting, transfer faults, and structural control of magmatic and hydrothermal processes in the TAG area, Mid-Atlantic Ridge 26°N. *Geol. Soc. Am. Bull.*, 102:1635–1645.
- Kleinrock, M.C., Humphris, S.E., and the Deep-TAG Team, 1996. Detailed structure and morphology of the TAG active hydrothermal mound and its geotectonic environment. In Humphris, S.E., Herzig, P.M., Miller, D.J., et al., *Proc. ODP, Init. Repts.*, 158: College Station, TX (Ocean Drilling Program), 15–21.
- Krasnov, S., Stepanova, T., and Stepanov, M., 1994. Chemical composition and formation of a massive sulfide deposit, Middle Valley, northern Juan de Fuca Ridge (Site 856). In Mottl, M.J., Davis, E.E., Fisher, A.T., and Slack, J.F. (Eds.), *Proc. ODP, Sci. Results*, 139: College Station, TX (Ocean Drilling Program), 353–372.
- Lalou, C., Reyss, J.-L., Brichet, E., Rona, P.A., and Thompson, G., 1995. Hydrothermal activity on a 10⁵-year scale at a slow-spreading ridge, TAG hydrothermal field, Mid-Atlantic Ridge 26°N. *J. Geophys. Res.*, 100:17855–17862.
- Mills, R.A., and Elderfield, H., 1995. Rare earth element geochemistry of hydrothermal deposits from the active TAG mound, 26°N Mid-Atlantic Ridge. *Geochim. Cosmochim. Acta*, 59:3511–3524.
- Rona, P.A., and Von Herzen, R.P., 1996. Introduction to special section on measurements and monitoring at the TAG hydrothermal field, Mid-Atlantic Ridge 26°N, 45°W. *Geophys. Res. Lett.*, 23:3427–3430.
- Shipboard Scientific Party, 1992. Site 856. In Davis, E.E., Mottl, M.J., Fisher, A.T., et al., *Proc. ODP, Init. Repts.*, 139: College Station, TX (Ocean Drilling Program), 161–281.
- _____, 1998. Middle Valley: Bent Hill Area (Site 1035). In Fouquet, Y., Zierenberg, R.A., Miller, D.J., et al., *Proc. ODP, Init. Repts.*, 169: College Station, TX (Ocean Drilling Program), 35–152.

Tivey, M., Humphris, S.E., Thompson, G., Hannington, M.D., and Rona, P.A., 1995.
Deducing patterns of fluid flow and mixing within the TAG active hydrothermal
mound using mineralogical and geochemical data. *J. Geophys. Res.*, 100:12527–
12555.

Figure F1. Location map of Middle Valley on the Juan de Fuca Ridge (modified from Davis, Mottl, Fisher, et al., 1992).

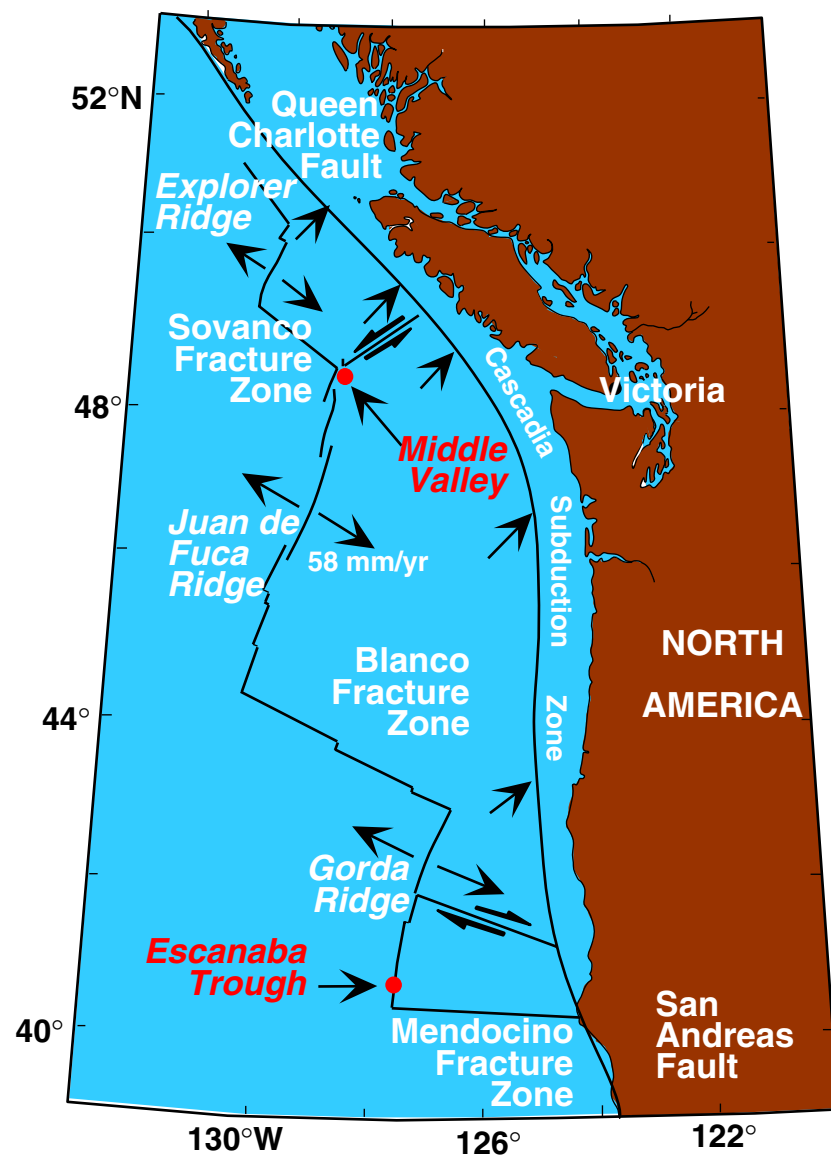


Figure F2. Plan view of the Bent Hill Massive Sulfide (BHMS) and ODP Mound deposits. Solid circles indicate locations of holes drilled during Leg 169 to define two orthogonal cross sections (modified from Fouquet, Zierenberg, Miller, et al., 1998).

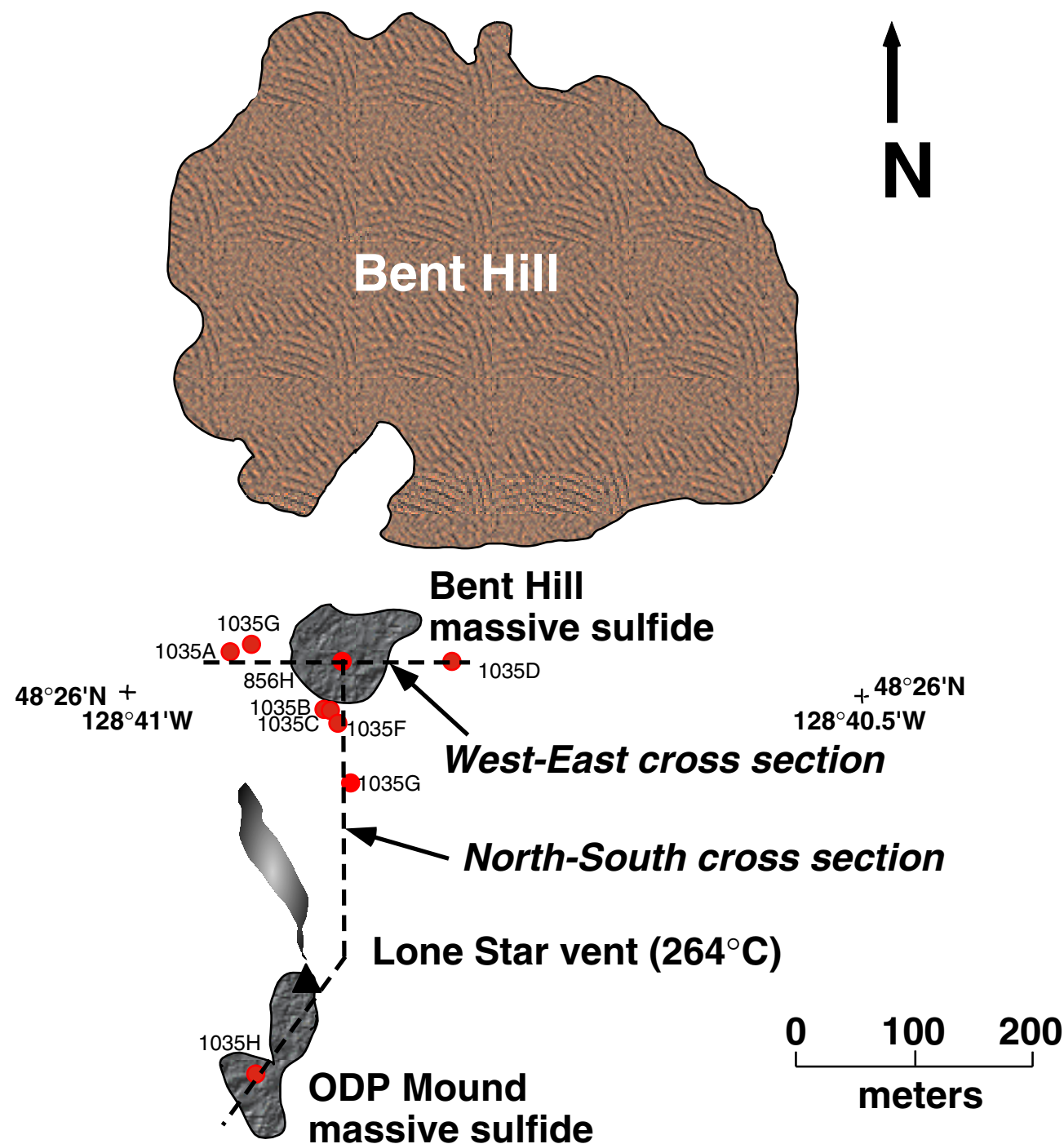


Figure F3. Schematic box diagram showing the stratigraphy of the BHMS and ODP Mound deposits. Stratigraphic control is based on boreholes. The relative locations of these boreholes is indicated by the solid circles along the seafloor surface and highlighted in the subsurface by brighter hues. The gray schematically shows hydrothermal plumes from vents created by drilling into the hydrothermal reservoir.

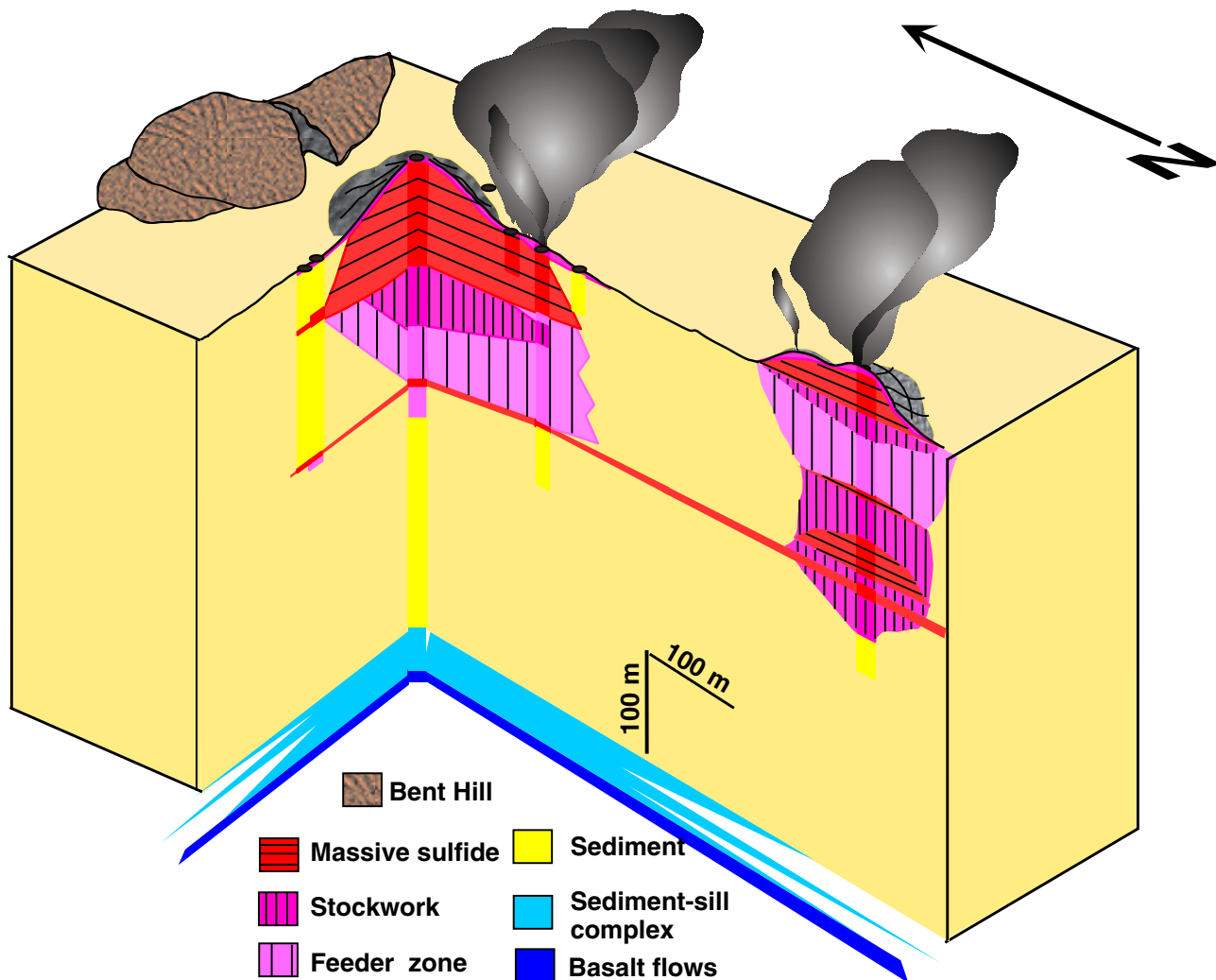


Figure F4. Location map of drill sites (TAG-1 through TAG-5) on the TAG hydrothermal mound. Inset shows the location of the TAG mound on the Mid-Atlantic Ridge (modified from Humphris, Herzig, Miller, et al., 1996). The letters A through Q represent locations of Site 957 drill holes.

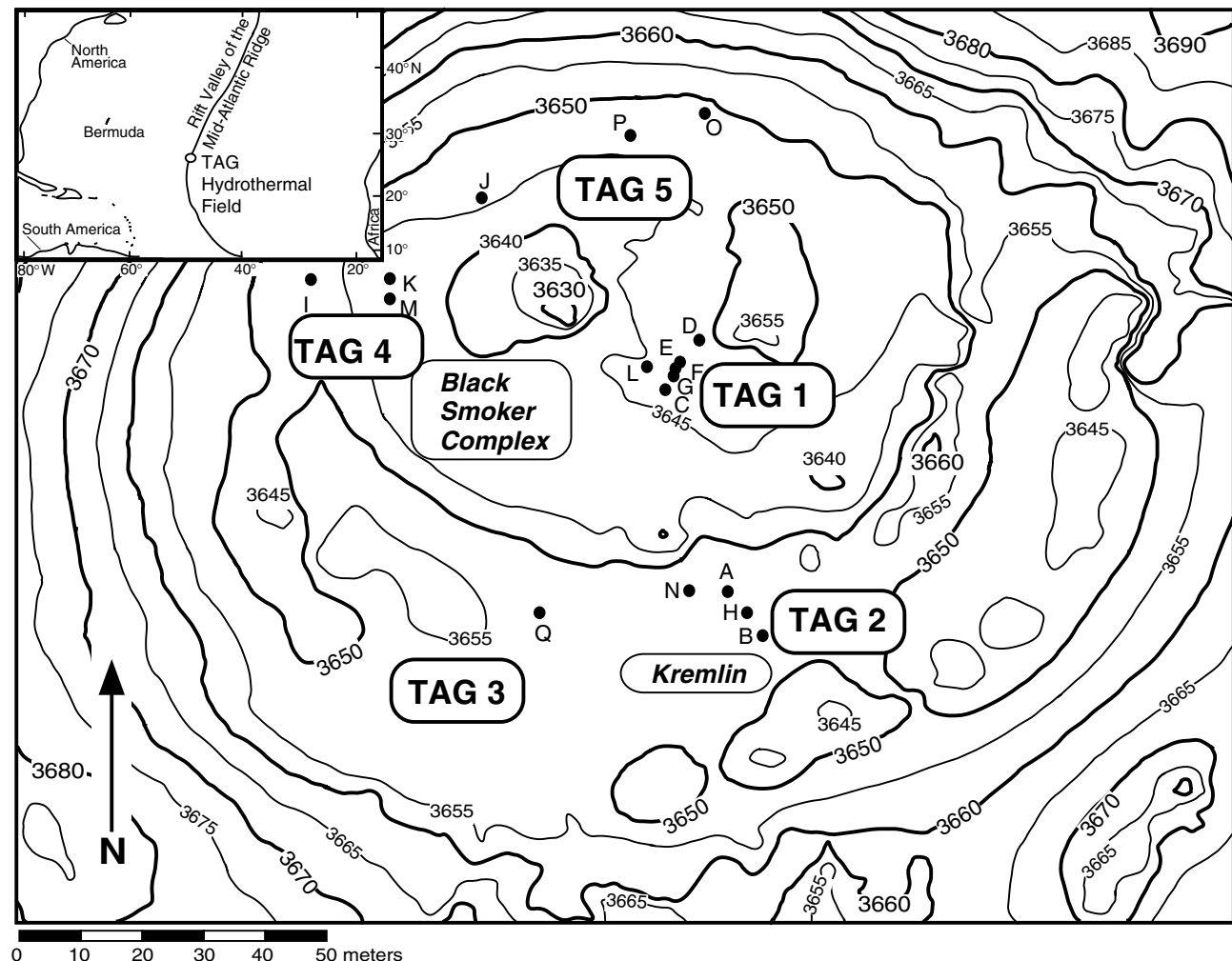


Figure F5. Schematic box diagram showing the stratigraphy of the TAG hydrothermal mound. Stratigraphic control is based on boreholes as identified in Figure F4, p. 13. The relative locations of the boreholes on the mound surface are indicated by the solid circles.

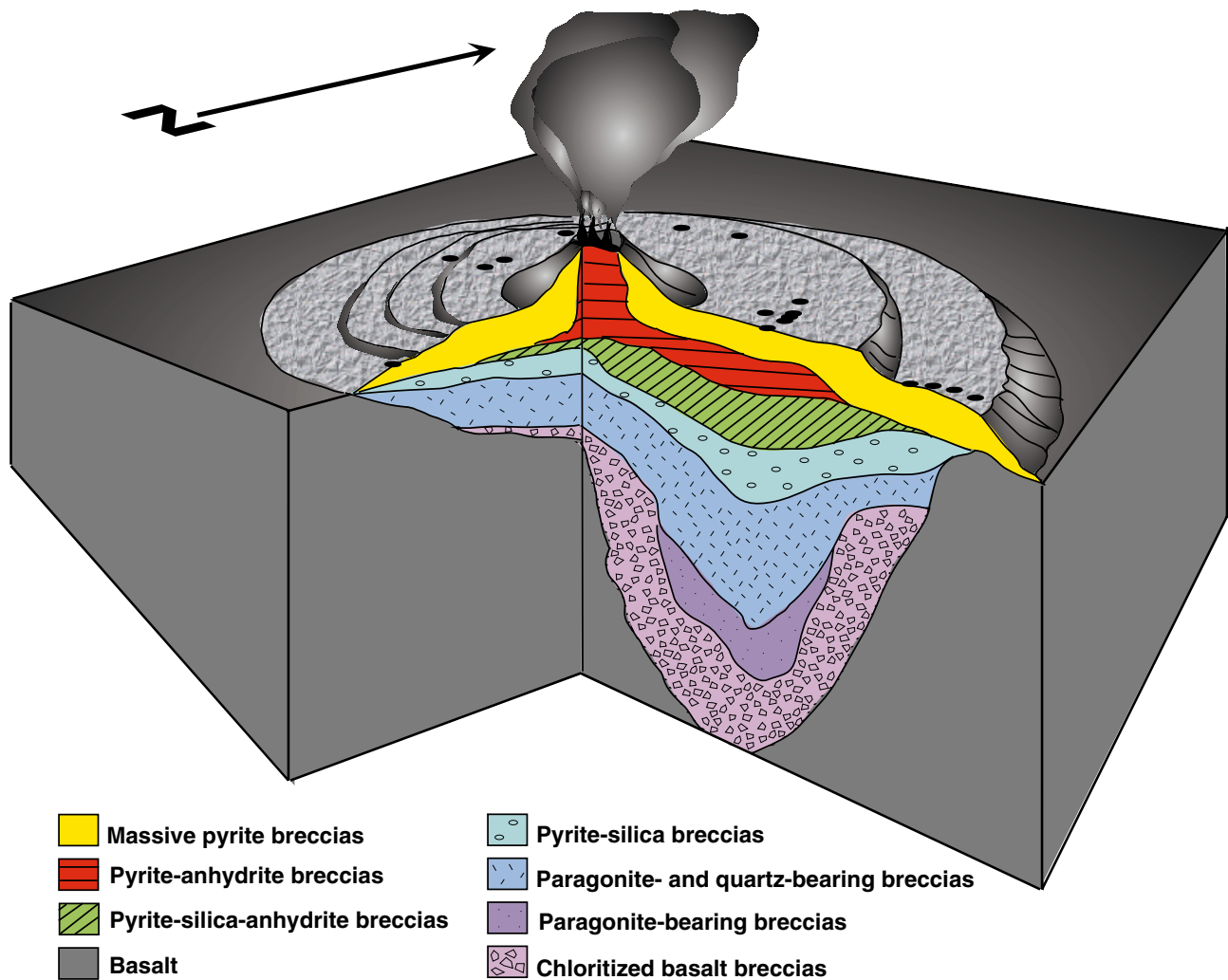


Figure F6. Changes in sulfide mineral and magnetite concentration (total ore mineral abundance normalized to 100%) relative to depth in Hole 856H (Bent Hill Massive Sulfide deposit). MGT = magnetite, SPH = sphalerite, PO = pyrrhotite, HM = hematite, PY = pyrite, MAR = marcasite, CPY = chalcopyrite, ISO = isocubanite. Data are compiled from Shipboard Scientific Party (1992), Shipboard Scientific Party (1998), Krasnov et al. (1994), and this study.

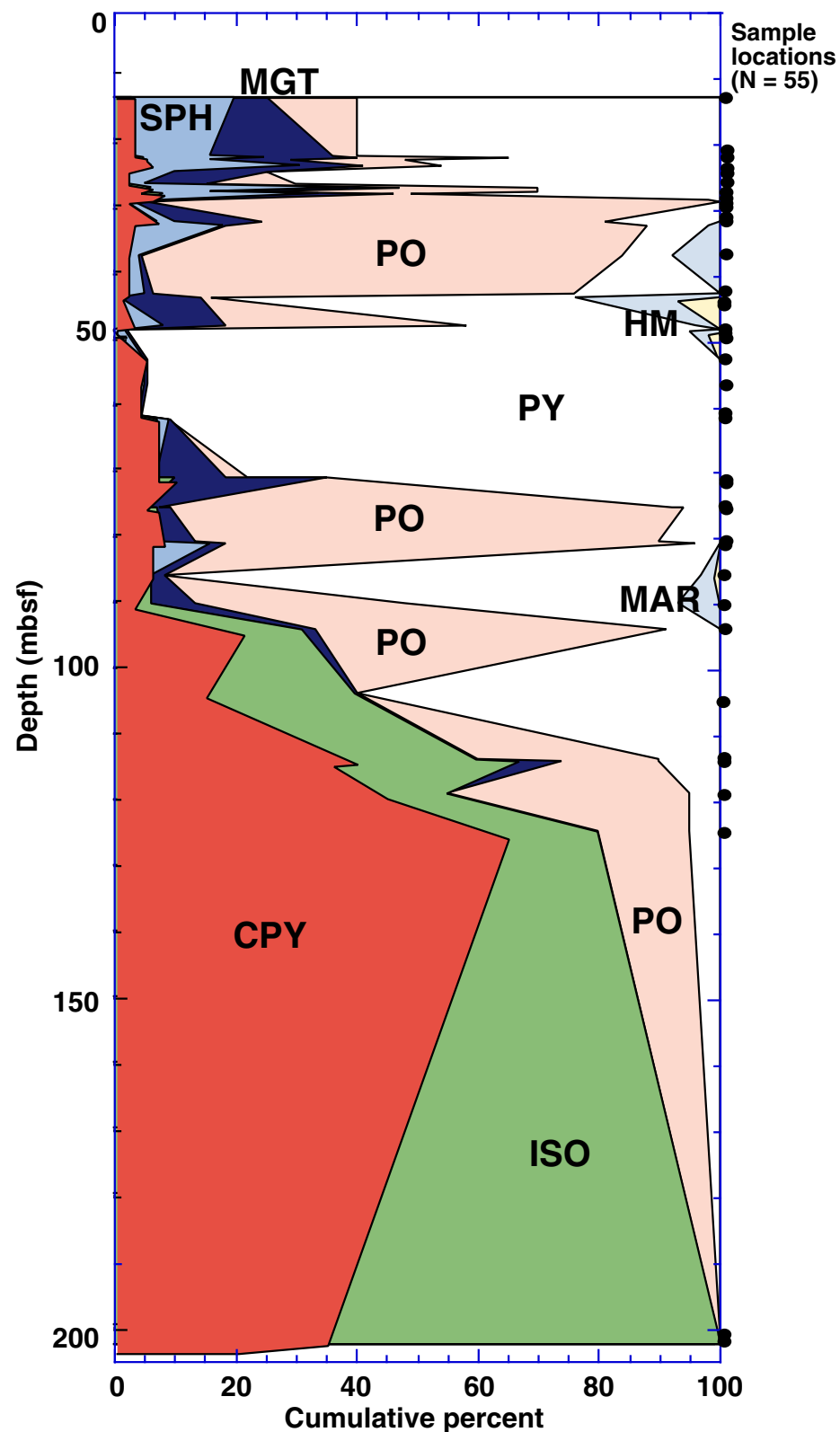


Figure F7. Reflected-light photomicrographs of (A) Sample 169-856H-31R-2, 1–5 cm, from the Deep Copper Zone beneath Bent Hill Massive Sulfide deposit, (B) Sample 169-1035H-19R-1, 58–62 cm, from the Deep Copper Zone beneath ODP Mound, and (C) Section 169-856H-19R-1, at 94 mbsf, ~100 m higher in the stratigraphy than the Deep Copper Zone at the base of the massive sulfide deposit. The host mineral is isocubanite, and the lamellae are chalcopyrite.

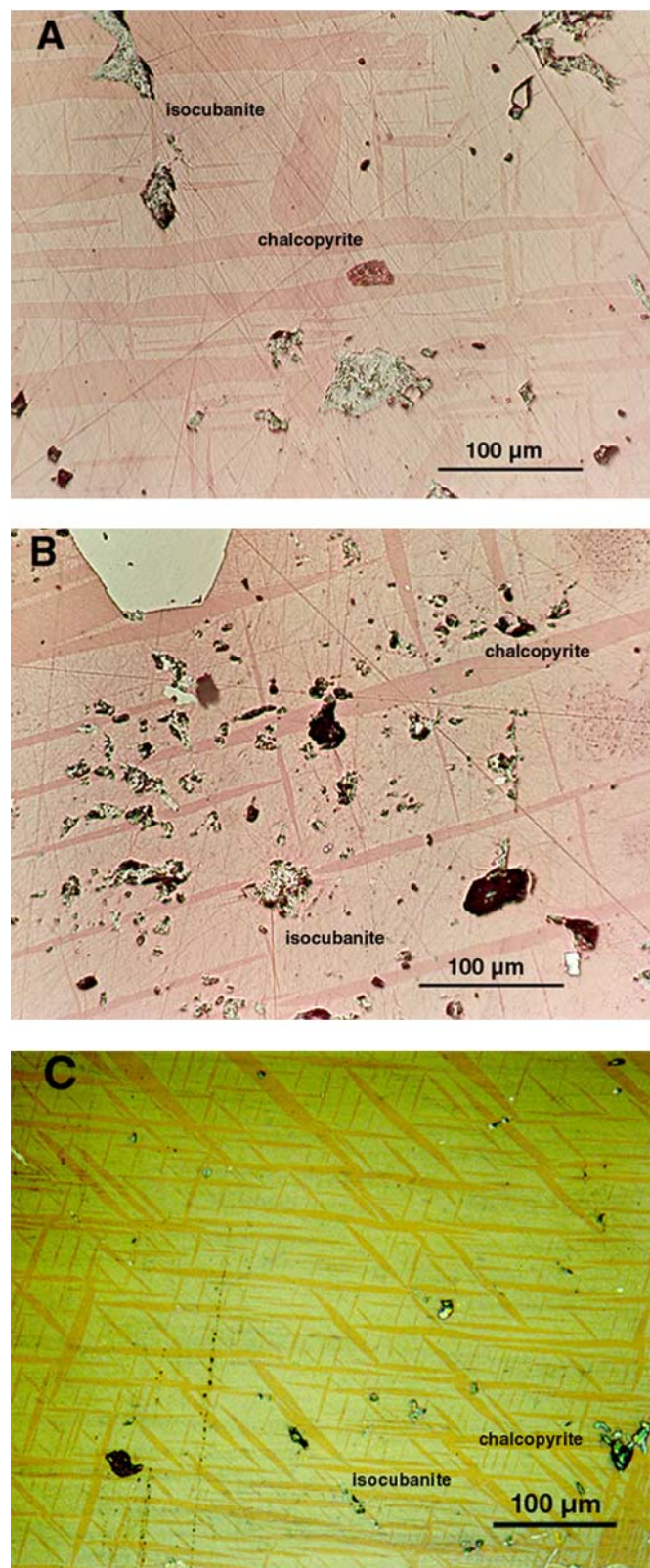


Figure F8. Reflected-light photomicrographs showing examples of chalcopyrite disease in sphalerite. All examples are from Section 169-1035H-16R-2. A. Two adjacent sphalerite grains (light). The grain on the right has rare chalcopyrite inclusions (darker gray in black-and-white image, pink hue in color). The grain on the left shows a more advanced stage of chalcopyrite exsolution. B. A vein of chalcopyrite is partially mimicking a grain boundary in sphalerite that is otherwise indistinct. C. This sphalerite has a dense array of subrounded to subangular chalcopyrite inclusions, and some groups of inclusions appear to be aligned and concentric, potentially marking crystal growth bands.

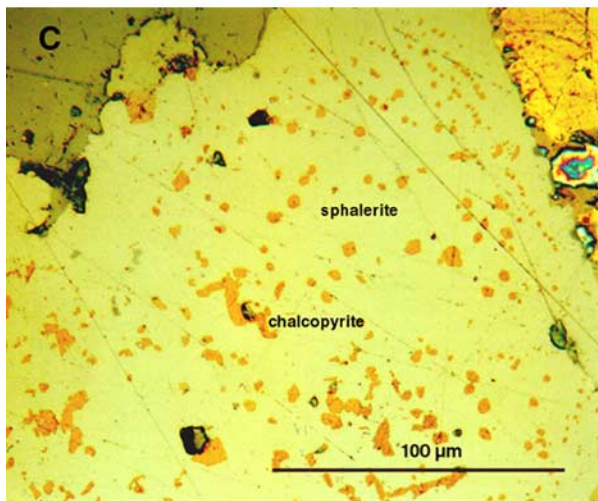
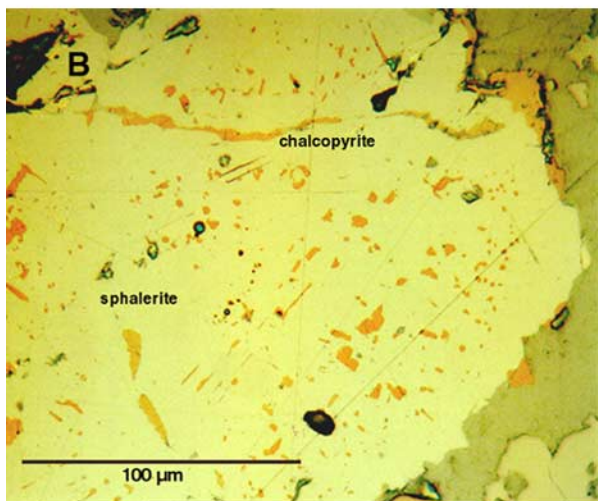
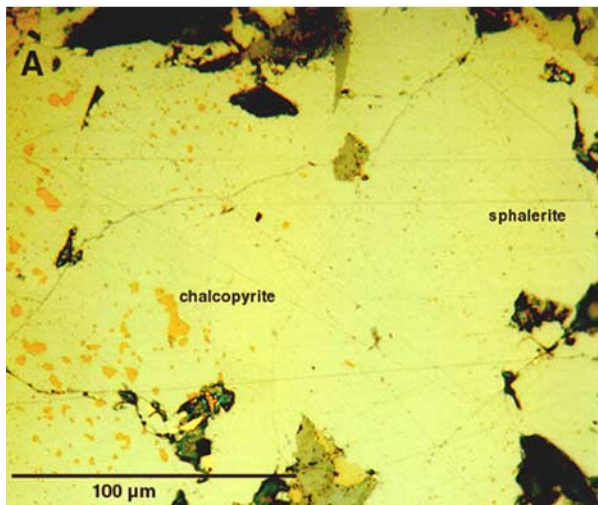


Figure F9. Reflected-light photomicrographs illustrating paragenetic relationships (see “Results and Discussion,” p. 5) in samples from ODP Mound massive sulfides. A–D. Sample 169-1035H-16R-2, 122–126 cm. E. Sample 169-1035H-2R-1, 32–36 cm. F. Sample 169-1035H-2R-2, 55–61 cm.

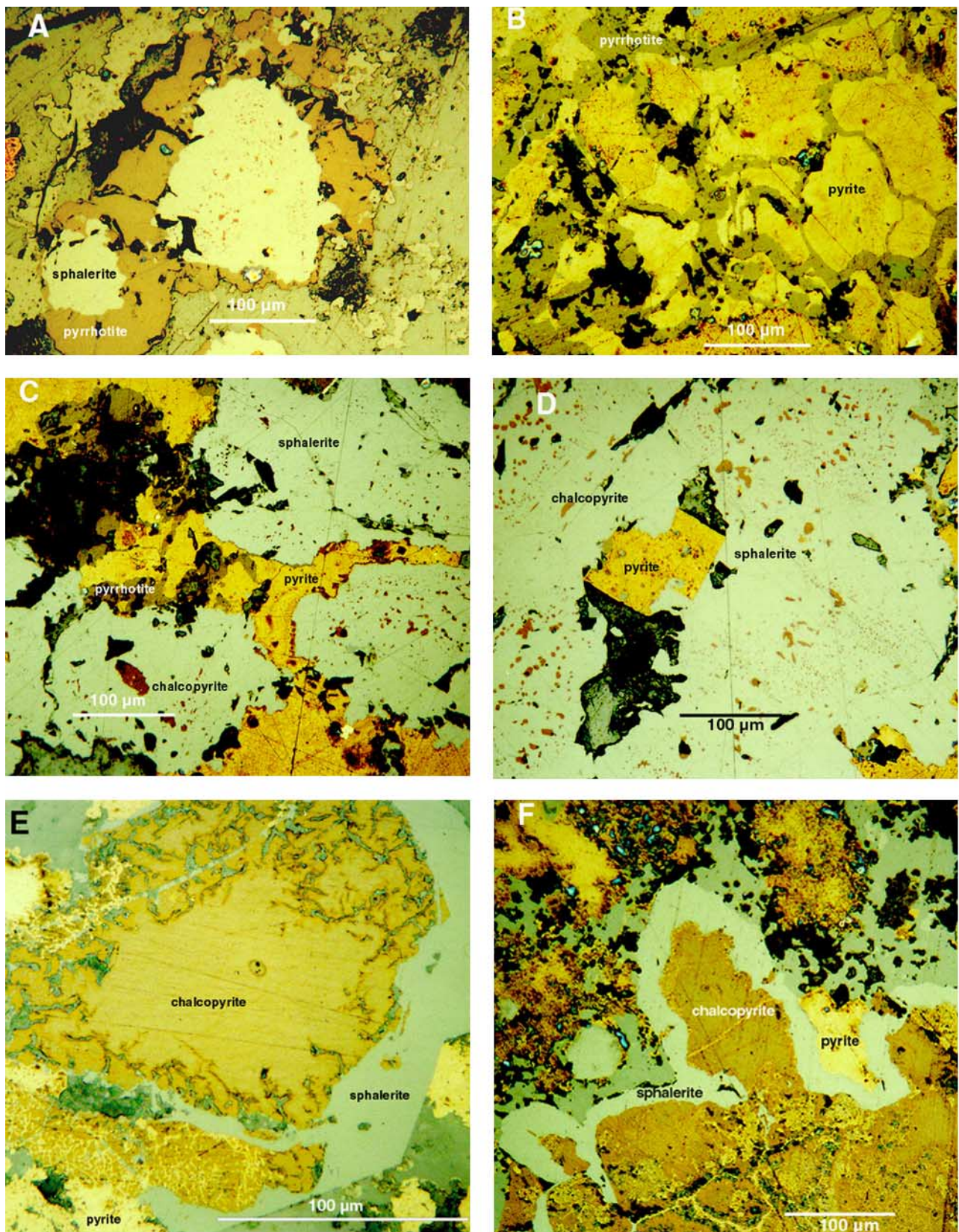
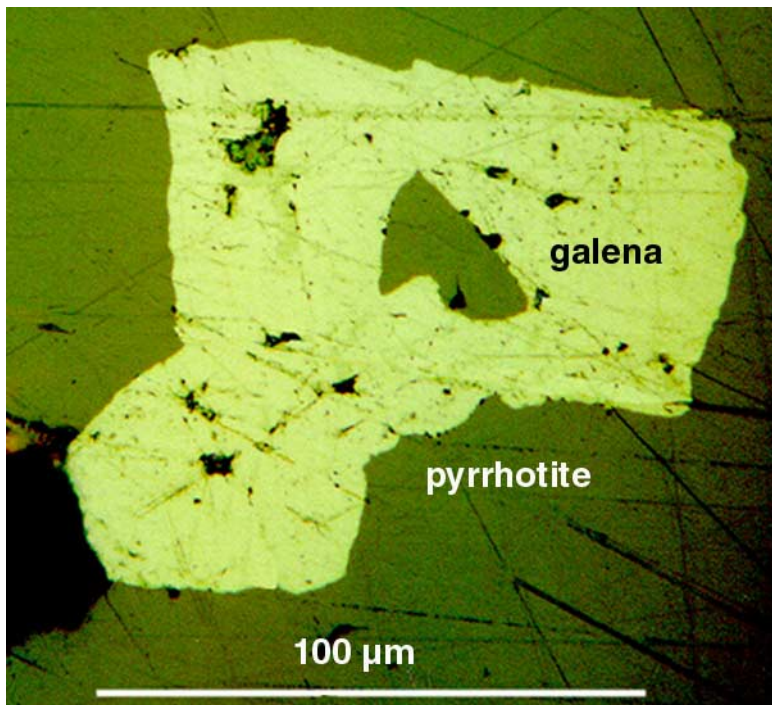


Figure F10. Reflected-light photomicrograph of euhedral galena inclusion in sphalerite (Sample 169-1035H-17R-1, 48–52 cm) from the ODP Mound.



D. LAWRIE AND D.J. MILLER
DATA REPORT: SULFIDE MINERAL CHEMISTRY AND PETROGRAPHY

23

Table T2 (continued).

Location	Core, section, interval (cm)	Depth (mbsf)	N	As	S	Sb	Pb	Fe	Co	Ni	Cu	Zn	Total		
	158-957A- 3X-1, 56	10.56	2	0.03	34.61	0.00	0.10	30.36	0.00	0.00	34.35	0.08	99.53		
	158-957B- 3R-1, 3	14.93	<u>1</u> <u>13</u>	0.02	34.54	0.03	0.17	30.48	0.00	0.00	34.31	0.00	99.55		
TAG-5	158-957O- 2R-1, 22	8.11	<u>5</u> <u>73</u>	0.02	34.70	0.01	0.11	30.35	0.00	0.00	34.31	0.00	99.51		
			N	As	S	Mn	Sb	Au	Pb	Fe	Co	Ni	Cu	Zn	Total
	Average sphalerite compositions														
	TAG-1		6	0.01	33.37	0.01	0.00	0.02	0.05	2.62	0.00	0.01	0.39	63.48	99.96
	TAG-2		11	0.02	33.52	0.01	0.01	0.01	0.09	1.76	0.00	0.01	0.42	63.71	99.56

Notes: TAG = Trans-Atlantic Geotraverse. See Table T5, p.31, for the complete data set for the TAG hydrothermal mound.

